Sustainable and Cyclic Synthesis of 2D $Co(OH)_2$ Nanosheets for Scalable Production of High-Performance Electrocatalysts

*Ziyi Zhang, Corey Carlos, Derui Wang, Yutao Dong, Xudong Wang**

Department of Materials Science and Engineering, University of Wisconsin-Madison, Madison, Wisconsin 53706, United States.

*Email: xudong.wang@wisc.edu

Keywords: 2D nanomaterial; Cyclic synthesis; Sustainability; Ionic layer epitaxy, Electrochemical catalysis.

ABSTRACT

Ultrathin 2D nanomaterials with extremely large surface area and unique electrochemical properties are considered excellent electrocatalyst candidates for clean energy conversion and environmental applications. However, it is still challenging to prepare 2D catalysts through a scalable and sustainable process that may become suitable for industrial demands. Here, we reported a facile cyclic synthesis method of ultrathin 2D nanomaterials based on the ionic layer epitaxy. By repeatedly refreshing a surfactant monolayer on the solution surface, free-standing 2.2 nm thick hexagonal $Co(OH)_2$ nanosheets were obtained from the water surface at ambient conditions in multiple cycles. These nanosheets exhibited a consistently high OER performance with an average overpotential of 427.4 ± 5.3 mV at 10 mA cm^{-2}. Remarkably, hexagonal NSs could be obtained from a wide range of precursor concentrations which could enable over 84 cycles of synthesis on the same stock precursor solution. It will shed light on the design of autonomous and sustainable synthesis of 2D nanomaterials for advanced electrocatalysis development toward a clean future.

INTRODUCTION

Advanced electrocatalysis is considered a promising approach to the global desire for clean energy and environmental sustainability.[1-6] The design and synthesis of efficient and affordable electrocatalysts are essential to many electrochemical energy conversion and storage applications.[7, 8] In recent years, two-dimensional (2D) nanomaterials with monolayer or a-few-layer thickness have attracted great attention, because of their remarkably high surface area, rapid charge transfer, and versatile surface functionalization.[9-11] Thence, they have been widely applied in vast fields such as electronics, electrocatalysis, and energy storage with great prospects for future industries. Various methods are available for creating 2D materials either from top-down or bottom-up, including mechanical exfoliation,[12] liquid exfoliations,[13] physical and chemical vapor deposition,[14-17] and reactions in solution.[18] Despite significant progress and wide ranges of achievements, a few critical obstacles still restrict the field of large-scale preparation and applications of 2D catalysts. For example, top-down methods such as exfoliation processes require long-time and energy-intensive sonication and centrifuge, with limited control over the size and geometry.[19, 20] In a large number of bottom-up methods studied to date, 2D nanomaterials synthesis mainly relies on high vacuum physical or chemical deposition,[15] or high temperature and pressure-based solvothermal methods.[21] Both approaches are also limited to naturally layered materials, i.e. van der Waals solids. In addition, these approaches are often associated with expensive equipment, hazardous chemicals, and high energy and materials consumptions. These largely impede the application of 2D nanomaterials from meeting the industrial demands, where the materials and synthesis process should be scalable, cost-effective, and environmental-friendly.[22] Recently, we developed a solution-based approach, ionic layer epitaxy (ILE) to synthesizing 2D materials from a wide range of materials including metals, oxides, and hydroxides beyond the limitation of van der Waals solids.[23-29] This technique relies on the ionized surface monolayer to serve as a floating substrate, which directs the growth of nanometer-thick 2D nanosheets (NSs) underneath. By tuning the electrical double layer at the interface, ILE is able to adjust the thickness of NSs within the 1 nm regime. Precise control of the thickness enables a fine-tune of the NSs' physical and chemical properties, including electronic bandgap, conductivity, and catalytic. Therefore, compared to other conventional 2D nanomaterials synthesis methods, ILE excels in simplicity, using readily available sources and tools, which translates into significantly

lower costs, easier scale-up and broader industrial potential - a sustainable, cost-effective and accessible alternative to conventional methods.

Here, we report a sustainable and cyclic synthesis strategy for growing 2D nanomaterial at the air-water interface based on ILE. Nanometer-thick nanosheets (NSs) were successfully synthesized via ILE over multiple cycles from a repeatedly used aqueous solution containing tartrate-coordinated[30, 31] metal precursor ions at ambient conditions. After the free-standing 2D materials were transferred, the remaining precursor solution could be reused by adding a new layer of surfactants. In addition, the used surfactants could be recycled by organic solvent extraction.[32] All $Co(OH)_2$ NSs obtained 5 times from this cyclic ILE process demonstrated a consistent and outstanding oxygen evolution reaction (OER) performance. This strategy demonstrated the potential of scalable 2D materials synthesis with minimal waste source materials. This may open a new avenue for industrial-level production of 2D nanomaterials, which is sustainable and eco-friendly.

RESULTS AND DISCUSSION

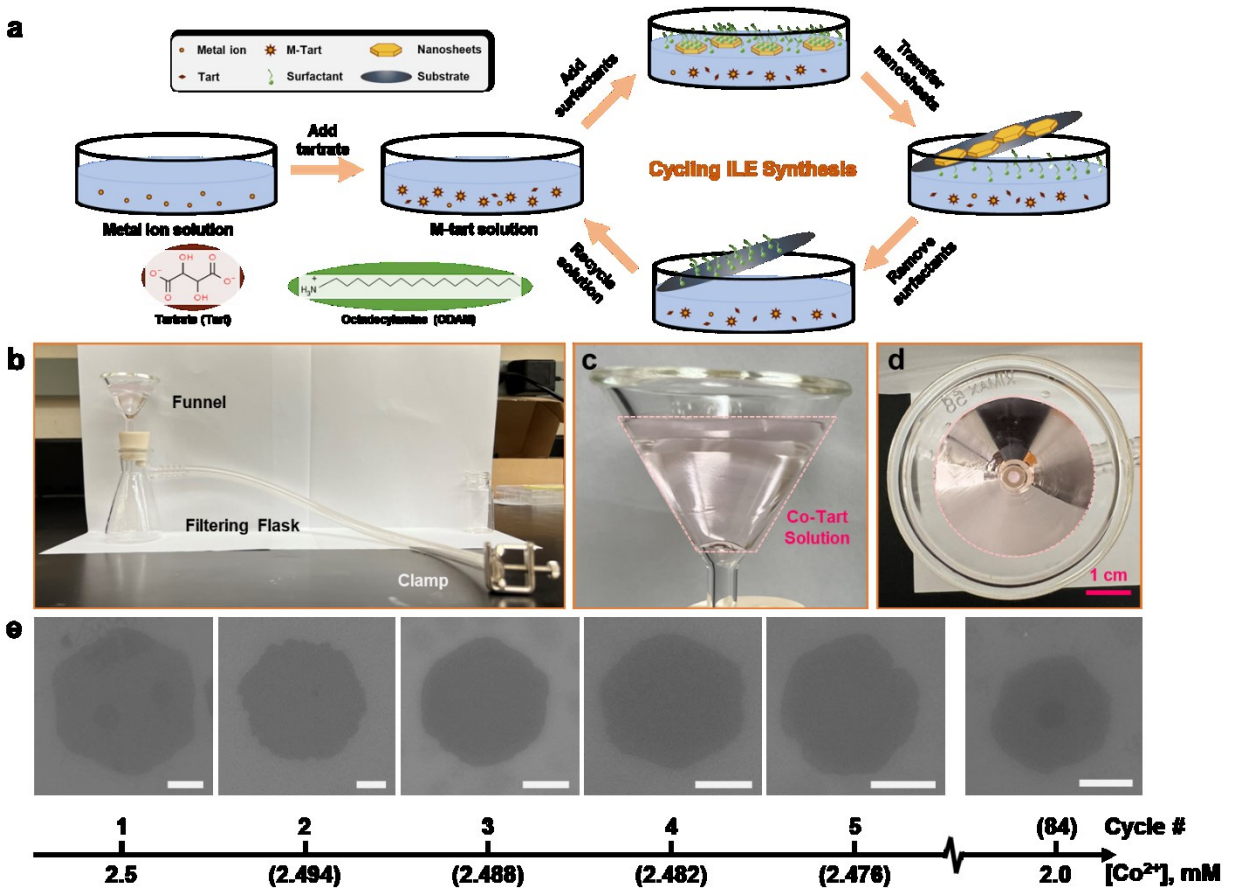

Figure 1. (a) Schematic illustration of the cycling ILE synthesis process. (b) Optical photo of the synthesis setup. (c) Co-Tart precursor solution in the synthesis funnel. (d) Stable air-water interface during ILE NS growth. (e) SEM images of $Co(OH)_2$ NSs from the cycling synthesis cycles. Numbers in parentheses are estimated. [scalebar = 1 μm]

The cyclic synthesis of 2D $Co(OH)_2$ was modified from a typical ILE process as reported,[23] and schematically illustrated in **Figure 1a**. A cobalt chloride ($CoCl_2$) aqueous solution was prepared as the precursor source. Additional ammonium tartrate ($(NH_4)_2$Tart) was introduced to coordinate the metal ion for enhanced solution stability.[30, 31, 33] Tartrate molecules with two anionic carboxyl groups not only formed a complex (Co-Tart) with metal ions[34, 35] to prevent the nucleation in bulk solution, but they also promoted the precursor accumulation at the cationic surfactant monolayer for the 2D crystal nucleation. To start the ILE synthesis, a chloroform solution containing octadecylamine (ODAM) was dropped cast on the water surface. A monolayer of positive charged ODAM assembled at the air-water interface with

a theoretical density of 1.6 nmol cm^{-2} after chloroform was fully evaporated. Meanwhile, Co-Tarts were attracted to the ODAM monolayer forming an electrical double layer, where a few nm thick $Co(OH)_2$ NSs started to nucleate and grow after the superstation was reached.[36, 37] The growth of $Co(OH)_2$ NSs finished in 4 hours, and they were transferred to an supporting substrate by scooping from the water surface. Given the NS thickness was confined by the electrical double layer, only a few nm-deep region at the water-air interface was involved in the NS growth,[25, 26, 38]only a trace-level amount (on nano-molar magnitude) of precursors was converted to NSs from the solution. [39]Based on the ILE mechanism, this synthesis process can be repeated after removing the disturbed surfactants and rebuilding a new surfactant monolayer.

To demonstrate the sustainability of the cyclic ILE synthesis, a facile "funnel + filtering flask" setup was developed to collect the NSs, remove residue surfactants and recycle the precursor solution (**Figure 1b, see Method for experimental details**). During the NS synthesis, the clamp was closed, and the solution was held steady in the funnel by the air pressure (**Figure 1c**). Adding 10 mL solution gave a consistent opening area with a diameter of about 3 cm in the funnel (**Figure 1d**). The pink color of the precursor solution (2.5 mM) did not visibly fade after synthesis suggesting that there was a substantial amount of precursors remaining in the post-synthesis solution. Based on the experimental procedure, we estimated the cobalt precursor consumption from one ILE NS synthesis and further predicted the upper limit of the number of cycles that may be achieved by this synthesis strategy. Assuming the air-water interface was fully covered by $Co(OH)_2$ NSs with a uniform 2.2 nm thickness, approximately 60.2 nmol Co^{2+} would be consumed in one synthesis, equivalent to a 0.006 mM drop for 10 mL solution. This 0.24% concentration drop had negligible influence on reuse for synthesizing the NS again.

To show the cyclic ability, the $Co(OH)_2$ NSs were synthesized using this setup and repeated five times. During all five synthesis cycles, the precursor solution remained a light pink color of the Co-Tart complex, and showed no Tyndall effect as the laser passed through, suggesting no particles formed in the bulk solution (**Figure S1a**). Scanning electron microscopy (SEM) demonstrated that all the NSs exhibited the same hexagonal morphology with a 3 μm lateral size (**Figure 1e**). No particles or other nanostructures were observed from the collected samples, and only the coverage varied slightly due to the fluctuation of imprecise surfactant density between cycles (**Figure S1b**). The NSs were evenly distributed on the surface as a single layer with a coverage of about 26% without apparent overlaps. After the NSs were transferred from the fifth

synthesis cycle and ODAM was removed, the possible residues on the flask-collected post-synthesis solution surface were scooped on the Si substrate and characterized by SEM (**Figure S2a**). No obvious particles or micelles were found, suggesting that surfactants were successfully removed, and the recycled solution could be further used for more synthesis cycles. To further show the negative effect of leftover surfactant at the air-water interface, the fresh precursor solution after adding surfactants was collected by the bottom flask without the surfactant removal step. Then, this solution was reused for another synthesis. Under a non-uniform surfactant layer, no NSs were obtained after 4-hour synthesis. Only nanoparticle agglomerations were gained from the air-water interface (**Figure S2b**). These results suggested that completely removing surfactant residue after every synthesis is vital because NSs prefer to grow under a uniform surfactant monolayer.

It is non-trivial to make an obvious solution concentration reduction by repeating the synthesis process because the concentration drop was estimated as only 0.006 mM per synthesis cycle. Instead, we carried out a synthesis of 2 mM Co^{2+} precursor solution with other parameters the same, to present the repeatability at low precursor concentration (As calculated, the initial Co^{2+} concentration for the 84th synthesis cycle would be 2 mM). The hexagonal NS morphology persisted with a moderately shorter edge length (**Figure 1e**). This suggested that the Co^{2+} concentration window for this hexagonal NSs growth is wide, potentially allowing over 84 synthesis cycles with careful operations. The precursor ions in the solution can be efficiently utilized for the synthesis, and this cycling process is promising for a sustainable 2D material preparation.

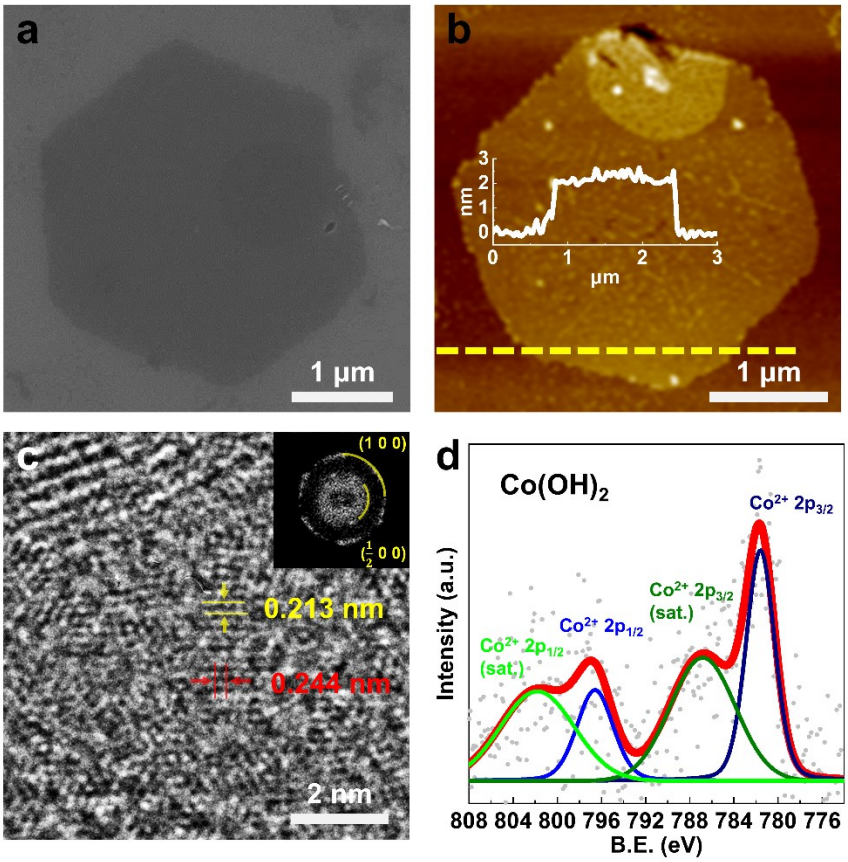

Figure 2. $Co(OH)_2$ NSs Characterizations. (a) SEM image; (b) AFM topography of hexagonal NSs. (c) HRTEM image with FFT. (d) XPS Co 2p spectrum.

More characterizations were performed on the hexagonal $Co(OH)_2$ NSs. As shown in **Figure 2a**, The $Co(OH)_2$ NS synthesized from a fresh solution possessed a hexagonal shape with a lateral size of 3 μm. The NSs were evenly distributed on the surface as a single layer with a coverage of about 26% without apparent overlaps **(Figure S1b)**. Atomic Force Microscopy (AFM) further revealed the flat surface of the hexagonal NS and the uniform thickness of 2.2 nm with a roughness of 0.2 nm (**Figure 2b**). HRTEM also evidenced the hexagonal lattice structure of β-$Co(OH)_2$ with (001) plane exposed. The lattice spacing of 0.213 and 0.244 nm were associated with the (110) and (100) atomic planes,[40] respectively (**Figure 2c**). X-ray photoelectron spectroscopy (XPS) spectra were obtained to analyze the chemical states (**Figures 2d and S3**). The Co $2p_{3/2}$ and Co $2p_{1/2}$ peaks located at 181.6 and 796.6 eV, respectively, which were attributed to the Co^{2+} oxidation state in the β-$Co(OH)_2$ phase. The ultrathin flat morphology of these $Co(OH)_2$

NSs with large surface exposure of Co sites makes them suitable for highly efficient electrocatalytic applications.

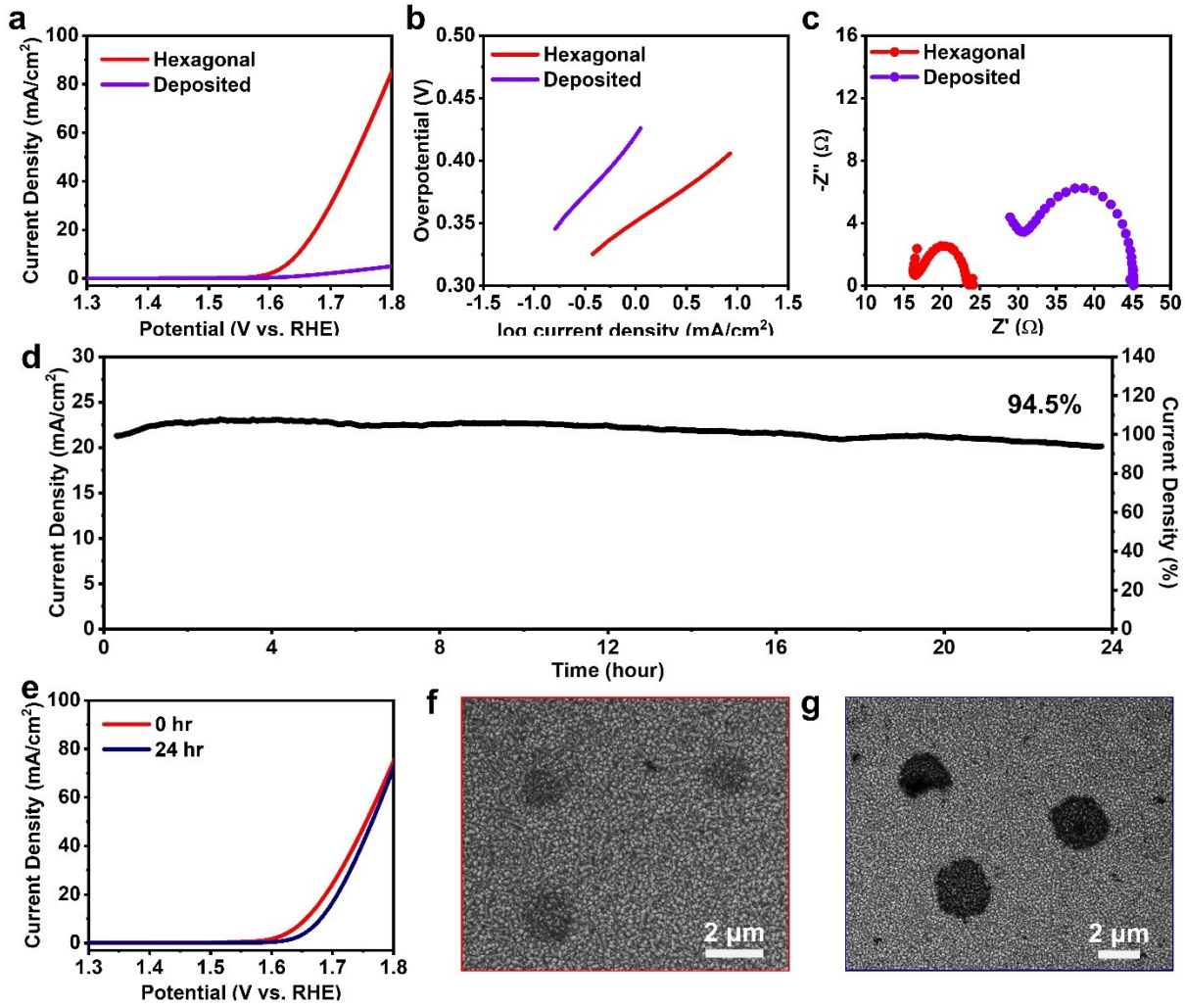

Figure 3. OER performance of $Co(OH)_2$ NSs from the first cycle ILE synthesis. (a) LSV curves; (b) Tafel slopes; (c) Nyquist plots; (d) 24-hour CA curve of hexagonal $Co(OH)_2$ NSs (@1.72 V vs. RHE). (e) LSV before and after 24 hours test. SEM images of $Co(OH)_2$ NSs on FTO substrates (f) before and (g) after the stability test.

The OER catalytic properties of these $Co(OH)_2$ NSs were then investigated by electrochemical measurements. Fluorine-doped tin oxide (FTO) substrates were used as working electrodes, and all measurements were carried out in 1M KOH electrolyte with a three-electrode system. Because of the rough FTO surface, the distribution of surface water film after transfer was

largely disrupted. Consequently, the NSs distribution on the FTO substrates showed a much lower uniformity compared to those on the Si substrates. This also brought challenges to precisely quantify the surface coverage of NS on FTS substrates. However, the yield of NS on water surface would not be impacted. Therefore, the NS coverage (26%) determined on Si substrate under the same synthesis conditions was used here to estimate the current density. Electrochemically deposited $Co(OH)_2$ NSs on FTO were made as a reference to show the enhanced catalytic properties of the as-synthesized hexagonal NSs from the ILE method (**Figure S4**). As the linear sweep voltammetry (LSV) curves shown in **Figure 3a**, the deposited NSs showed an onset potential of 329 mV vs. the reversible reference electrode (RHE), and the hexagonal NSs obtained from the first cycle showed a lower onset potential of 307 mV vs. RHE. In comparison, the deposited NSs could only produce a current density of 0.947 mA cm^{-2} at an overpotential of 416 mV vs. RHE. At the same overpotentials of 416 mV vs. RHE, the hexagonal NSs were able to achieve a current density of 10 mA cm^{-2}, which was 10.6 times larger than that of deposited NSs. The Tafel slopes were extrapolated and presented in **Figure 3b**. The Tafel slope of the deposited NSs was determined to be 91.0 mV dec^{-1}, and the Tafel slope of the hexagonal NSs was sharply reduced to 57.8 mV dec^{-1}, indicating the hexagonal NSs had faster interfacial kinetics compared to the deposited NSs. Similar surface kinetics were also revealed by the Nyquist plots (**Figure 3c**) obtained from electrochemical impedance spectroscopy (EIS). The semicircle represented the change transfer resistance between the catalyst and the electrolyte interface. The semicircle radius of the hexagonal NSs was about half smaller than that of deposited NSs, suggesting a significantly enhanced change in transfer kinetics across the electrode-electrolyte interface. In general, the 2D morphology could offer unique advantages including abundant surface active sites for binding reactants (**Figure S5**), and short charge transfer lengths between the electrode surface and electrolyte, making the hexagonal $Co(OH)_2$ NSs from ILE a superb OER catalyst.

Furthermore, the long-term stability of the $Co(OH)_2$ NSs from the first cycle was assessed via chronoamperometry (CA) at 1.72 V vs. RHE. Over 24 hours of continuous operation, 94.5% of current density was maintained (**Figure 3d**). Accordingly, the LSV curves after 24 hours exhibited an overpotential of 461 mV vs. RHE at 10 mA cm^{-2}, which was 24 mV higher than the initial value (**Figure 3e**). Consistently, the SEM characterizations of the NSs before and after the 24-hour CA measurements evidenced the good stability of the NSs (**Figure 3f-g**), despite the different contrasts indicating a conductivity decrease. The rough surface of the FTO substrate hindered water flow

uniformity compared to the smoother Si substrate. This disrupted the deposition of nanosheets (NSs), causing uneven coverage with scrambled or folded NSs. Consequently, the yield and uniformity of NSs on the FTO substrate were significantly lower than on the Si substrate. Because the catalysts often degrade during electrochemical water splitting, it is important to improve the stability by strategies like active site protection, catalytic carrier reinforcement and surface reconstruction. [41] Here we argue that the ultra-thin 2D morphology of NS can provide strong adhesion to the substrate and avoids detachment or possible mechanical damage. Therefore, this NS morphology can be more resistant to degradation compared to irregular or rough electrode surfaces, and more suitable for large-scale industrial-scale fabrication.

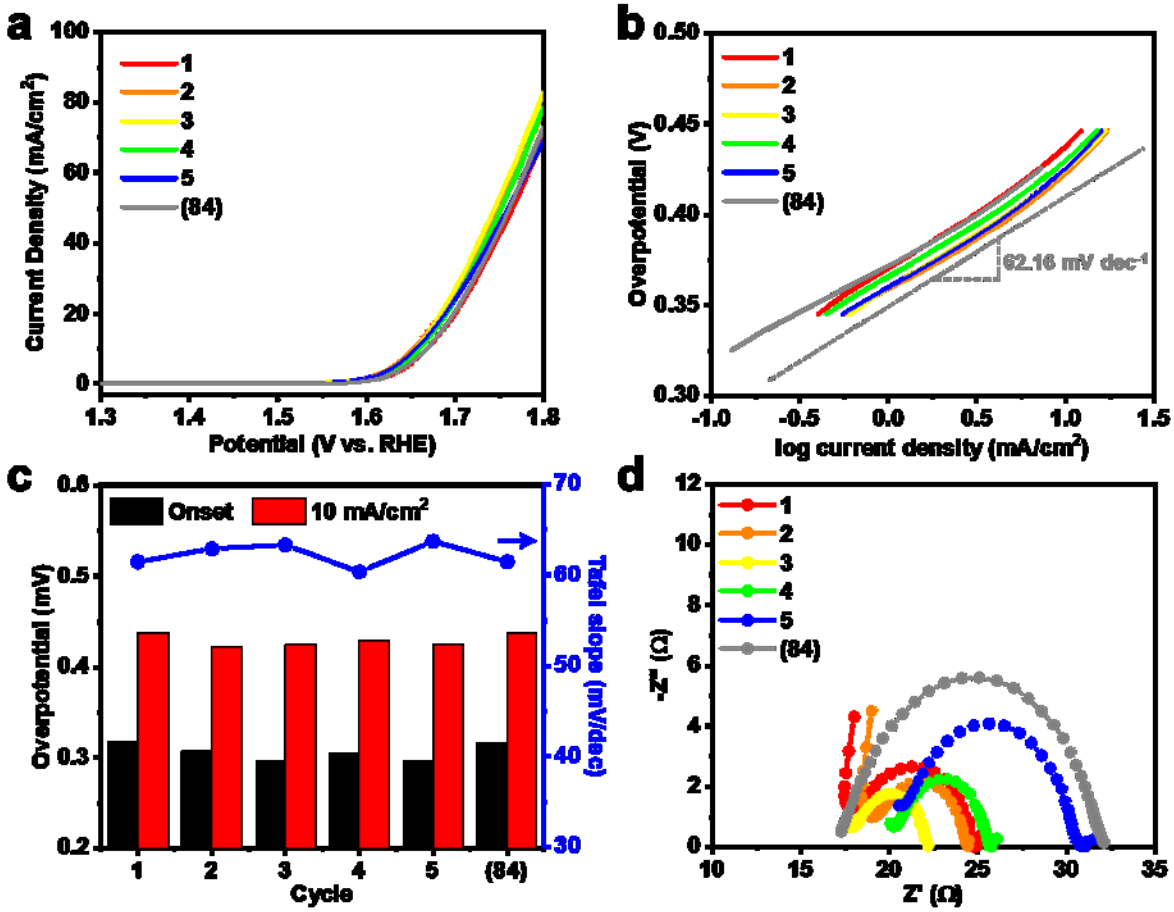

Figure 4. OER performance of $Co(OH)_2$ NSs from cycling synthesis. (a) LSV; (b) Tafel plots; (c) overpotentials and Tafel slopes; (d) Nyquist plots.

The electrochemical properties of $Co(OH)_2$ NSs from other repeating cycles were then investigated and compared to validate the cyclic synthesis capability. As the LSV curves shown in **Figure 4a**, all $Co(OH)_2$ NSs samples from the five cycles exhibited about the same performance with an average onset potential of 304.4 ± 7.6 mV vs. RHE and an average overpotential of 427.4 ± 5.3 mV vs. RHE at 10 mA cm^{-2}. The Tafel slopes extracted from the LSV curves are presented in **Figure 4b**. The OER kinetics for the five samples were also consistent, which revealed an average value of 62.16 ± 1.06 mV dec^{-1}. The variation over all samples was summarized in **Figure 4c** and compared with the NSs synthesized in a conventional non-cyclic glass container and the electrochemical deposited NSs in **Table 1**. The Nyquist plots from the EIS data revealed that the charge transfer resistances of the hexagonal NSs were much lower than the electrochemical deposited NSs (**Figures 3c and 4d**). Hexagonal NSs displayed a faster faradaic process and a higher electric conductivity at the electrode-electrolyte interface, which were contributed by their ultrathin thickness. The cycling synthesis demonstrated consistent high OER activities of the $Co(OH)_2$ NSs, confirming the success of the cycling ILE synthesis for scalable high-efficient 2D catalyst preparation. [41] The large contrast between nearly identical LSV curves and diverse EIS spectra in our cycled Co(OH)2 NSs was likely a result of the different probe depth between these two approaches, where LSV probes only surfaces , and EIS uncovers the property from the entire electrode landscape.. This phenomenon indicates the possible presence of bulk residues on 2D surfaces after long cycles of synthesis.

Table 1. OER performance of $Co(OH)_2$ NSs from cycling synthesis.

Cycle	Cobalt	Onset potential	Overpotential @10mA cm^{-2}	Tafel slope
	[mM]	[mV]	[mV]	[mV/dec]
In vial	**2.5**	**0.307**	**0.416**	**57.8**
Deposited	**NA**	**0.329**	**0.721**	**91.0**
1	**2.5**	**0.317**	**0.437**	**61.5**
2	**2.494**	**0.307**	**0.422**	**62.9**
3	**2.488**	**0.297**	**0.424**	**63.3**

4	**2.482**	**0.305**	**0.429**	**60.4**
5	**2.476**	**0.296**	**0.425**	**62.7**
(84)	**2.0**	**0.316**	**0.437**	**61.5**

CONCLUSIONS

In conclusion, we reported a facile cyclic synthesis method of ultrathin 2D NSs based on the ILE technique. Taking the unique advantages of the tartrate coordination in the solution and the charged surfactant monolayer at the surface, 2D crystal nucleation and growth were confined at the air-water interface. Free-standing 2.2 nm thick hexagonal $Co(OH)_2$ NSs were obtained from the water surface at ambient conditions and could be easily transferred to arbitrary substrates. We demonstrated that the morphology of $Co(OH)_2$ NSs could be well-preserved over five synthesis cycles and all the NSs showed superior OER performance due to their ultrathin thickness. They possessed an average overpotential of 427.4 ± 5.3 mV vs. RHE at 10 mA cm^{-2} with 94.5% retention after 24 hours. We estimated that this method may potentially achieve over 84 synthesis cycles with almost no waste generated. The cyclic synthesis design enables a potential for autonomous synthesis, for example, by adapting a Langmuir-Blodgett trough with robotic top bars to achieve automatic NS transfer and surfactant removal processes. This work reveals a scalable synthesis strategy of ultrathin 2D materials, presenting a promising solution for the development of a facile, low-cost, and sustainable strategy of 2D catalyst preparation toward clean energy and environmental applications.

MATERIALS AND METHODS

Cycling synthesis of $Co(OH)_2$ NSs in a glass funnel. The hexagonal $Co(OH)_2$ NSs were synthesized by the ionic layer epitaxy (ILE) method. A 10 mL aqueous solution containing 2.5 mM cobalt (II) chloride ($CoCl_2$) and 4 mM tartrate (Tart) was prepared by successively dissolving ammonium L-tartrate (Sigma-Aldrich) and $CoCl_2 \cdot 6H_2O$ (Sigma-Aldrich) powders. The solution was then transferred into the funnel with the clamp closed. The liquid flow was controlled by using a clamp to change the air pressure in the filter flask. The chloroform solution containing 1.8 mM octadecylamine (ODAM, Sigma-Aldrich) was slowly added to the surface of the precursor solution

to maintain the ODAM density of 1.6 nmol cm^{-2} at the air-water interface. The reaction maintained kept at ambient conditions for 4 h. The $Co(OH)_2$ NSs could be transferred to any substrate by scooping the solution surface or extracting the solution for characterization and device fabrication. Si substrates were used for NS characterization. To recycle the solution after synthesis, the clamp was opened to allow the solution to fall into the flask. Approximately the last 50 μL of post-synthesis solution in the funnel neck was sacrificed for surfactant removal. The solution collected in the flask was used as the precursor solution for the next synthesis using the same procedure.

Characterization of $Co(OH)_2$ NSs. A Zeiss LEO 1530 field emission scanning electron microscope (FESEM) was used to study the morphologies of the $Co(OH)_2$ NSs. Atomic force microscopy (AFM) tomography images were obtained using an XE-70 Park System. X-ray photoelectron spectroscopy (XPS) spectra were obtained using a Thermo Scientific K-alpha XPS instrument at a 400 μm spot size, with the flood gun turned on during the measurements.

Working Electrode Preparation. All working electrodes were prepared on fluorine-doped tin oxide (FTO) substrates with an exposed area of 1 cm^2 (1 cm by 1 cm). $Co(OH)_2$ NSs for electrochemical measurements were directly transferred to FTO substrates by deposition at the air-water interface. The electrochemically deposited $Co(OH)_2$ film was prepared by galvanostatically maintaining a current density of -0.25 mA cm^{-2} for 45 s in an aqueous plating solution containing 10 mM $Co(NO_3)_2 \cdot 6H_2O$ and 30 mM KNO_3. The resulting $Co(OH)_2$ films were rinsed with DI water and then dried in air at room temperature.

Electrochemical Measurements. The electrochemical measurements were performed on an Autolab PGSTAT302N station, using the three-electrode setup, with $Co(OH)_2$ NSs on FTO substrate as the working electrode, a Pt wire as the counter electrode, and a saturated calomel electrode (E_{SCE} = 0.241 V) as the reference electrode. The potential was swept from the open circuit in the positive direction at a scan rate of 50 mV s^{-1} for CV scans.

Active Sites Analysis. The ECSAs of all $Co(OH)_2$ NSs were determined by determining the double-layer capacitance (C_{DL}) from CV measurements at different scan rates (0.01 to 0.05 V s^{-1}) in the range -0.15 to 0.05 V vs. SCE (0.92 to 1.12 V vs. RHE; in the non-Faradaic region) in 1 M KOH solution. The C_{DL} was calculated from the slope of the plot of the double-layer charge current (i_{DL}, mA) vs. the scan rate (ν, V s^{-1}).[42] The ECSA was calculated using the equation: $ECSA = C_{DL}/C_S$, where C_S is the specific capacitance of the samples. Herein, C_S of 0.040 mF cm^{-2}

was used according to the previously reported value of metal oxide/hydroxide in an alkaline solution.[43]

ASSOCIATED CONTENT

Supporting Information.

Additional SEM images, XPS spectra, and electrochemical characterizations.

AUTHOR INFORMATION

Corresponding Author

Xudong Wang - Department of Materials Science and Engineering, University of Wisconsin-Madison, Madison, Wisconsin 53706, United States; E-mail: xudong.wang@wisc.edu

Notes

The authors declare no competing financial interest.

ACKNOWLEDGMENT

This work was primarily supported by the National Science Foundation DMR-2114931.

REFERENCES

[1] Z. Li, Y. Chen, T. Ma, Y. Jiang, J. Chen, H. Pan, W. Sun, 2D Metal-Free Nanomaterials Beyond Graphene and Its Analogues toward Electrocatalysis Applications, Advanced Energy Materials, 11 (2021) 2101202.
[2] F. Liu, L. Zhang, L. Wang, F. Cheng, The Electrochemical Tuning of Transition Metal-Based Materials for Electrocatalysis, Electrochemical Energy Reviews, 4 (2021) 146-168.
[3] H. Wang, B.-H. Chen, D.-J. Liu, Metal–Organic Frameworks and Metal–Organic Gels for Oxygen Electrocatalysis: Structural and Compositional Considerations, Advanced Materials, 33 (2021) 2008023.
[4] H. Adamu, Z.H. Yamani, M. Qamar, Modulation to favorable surface adsorption energy for oxygen evolution reaction intermediates over carbon-tunable alloys towards sustainable hydrogen production, Materials for Renewable and Sustainable Energy, 11 (2022) 169-213.
[5] T. Wang, X. Cao, L. Jiao, MOFs-Derived Carbon-Based Metal Catalysts for Energy-Related Electrocatalysis, Small, 17 (2021) 2004398.

[6] Y. Zhang, F. Gao, D. Wang, Z. Li, X. Wang, C. Wang, K. Zhang, Y. Du, Amorphous/Crystalline Heterostructure Transition-Metal-based Catalysts for High-Performance Water Splitting, Coordination Chemistry Reviews, 475 (2023).
[7] Y. Wang, M. Zhang, Y. Liu, Z. Zheng, B. Liu, M. Chen, G. Guan, K. Yan, Recent Advances on Transition-Metal-Based Layered Double Hydroxides Nanosheets for Electrocatalytic Energy Conversion, Advanced Science, (2023) 2207519.
[8] H. Xu, H. Shang, C. Wang, Y. Du, Low-Dimensional Metallic Nanomaterials for Advanced Electrocatalysis, Advanced Functional Materials, 30 (2020) 2006317.
[9] L. Li, Y. Xia, M. Zeng, L. Fu, Facet engineering of ultrathin two-dimensional materials, Chemical Society Reviews, 51 (2022) 7327-7343.
[10] F. Wang, X. Wang, Mechanisms in the solution growth of free-standing two-dimensional inorganic nanomaterials, Nanoscale, 6 (2014) 6398-6414.
[11] H. Zhang, Ultrathin two-dimensional nanomaterials, ACS nano, 9 (2015) 9451-9469.
[12] K.S. Novoselov, A.K. Geim, S.V. Morozov, D. Jiang, Y. Zhang, S.V. Dubonos, I.V. Grigorieva, A.A. Firsov, Electric Field Effect in Atomically Thin Carbon Films, Science, 306 (2004) 666-669.
[13] V. Nicolosi, M. Chhowalla, M.G. Kanatzidis, M.S. Strano, J.N. Coleman, Liquid Exfoliation of Layered Materials, Science, 340 (2013) 1226419.
[14] W. Yao, H. Liu, J. Sun, B. Wu, Y. Liu, Engineering of Chemical Vapor Deposition Graphene Layers: Growth, Characterization, and Properties, Advanced Functional Materials, 32 (2022) 2202584.
[15] L. Sun, G. Yuan, L. Gao, J. Yang, M. Chhowalla, M.H. Gharahcheshmeh, K.K. Gleason, Y.S. Choi, B.H. Hong, Z. Liu, Chemical vapour deposition, Nature Reviews Methods Primers, 1 (2021) 5.
[16] Q. Shi, K. Tokarska, H.Q. Ta, X. Yang, Y. Liu, S. Ullah, L. Liu, B. Trzebicka, A. Bachmatiuk, J. Sun, L. Fu, Z. Liu, M.H. Rümmeli, Substrate Developments for the Chemical Vapor Deposition Synthesis of Graphene, Advanced Materials Interfaces, 7 (2020) 1902024.
[17] Y. Zhang, D. Wang, C. Ye, F. Gao, Z. Li, Y. Du, Regulation of crystallinity and defects on CoNiRuOx nanocages for enhanced oxygen evolution reaction, Chemical Engineering Journal, 466 (2023).
[18] C. Tan, H. Zhang, Wet-chemical synthesis and applications of non-layer structured two-dimensional nanomaterials, Nature communications, 6 (2015) 1-13.
[19] Y. Li, X. Chen, Y. Sun, X. Meng, Y. Dall'Agnese, G. Chen, C. Dall'Agnese, H. Ren, S.-i. Sasaki, H. Tamiaki, X.-F. Wang, Chlorosome-Like Molecular Aggregation of Chlorophyll Derivative on Ti3C2Tx MXene Nanosheets for Efficient Noble Metal-Free Photocatalytic Hydrogen Evolution, Advanced Materials Interfaces, 7 (2020) 1902080.
[20] M. Alhabeb, K. Maleski, B. Anasori, P. Lelyukh, L. Clark, S. Sin, Y. Gogotsi, Guidelines for Synthesis and Processing of Two-Dimensional Titanium Carbide (Ti3C2Tx MXene), Chemistry of Materials, 29 (2017) 7633-7644.
[21] S. Cao, B. Shen, T. Tong, J. Fu, J. Yu, 2D/2D Heterojunction of Ultrathin MXene/Bi2WO6 Nanosheets for Improved Photocatalytic CO2 Reduction, Advanced Functional Materials, 28 (2018) 1800136.
[22] X. Zhang, Y. Wang, C. Liu, Y. Yu, S. Lu, B. Zhang, Recent advances in non-noble metal electrocatalysts for nitrate reduction, Chemical Engineering Journal, 403 (2021) 126269.

[23] F. Wang, J.-H. Seo, G. Luo, M.B. Starr, Z. Li, D. Geng, X. Yin, S. Wang, D.G. Fraser, D. Morgan, Nanometre-thick single-crystalline nanosheets grown at the water–air interface, Nature communications, 7 (2016) 1-7.
[24] Y. Wang, Y. Shi, Z. Zhang, C. Carlos, C. Zhang, K. Bhawnani, J. Li, J. Wang, P.M. Voyles, I. Szlufarska, Bioinspired synthesis of quasi-two-dimensional monocrystalline oxides, Chemistry of Materials, 31 (2019) 9040-9048.
[25] X. Yin, Y. Shi, Y. Wei, Y. Joo, P. Gopalan, I. Szlufarska, X. Wang, Unit Cell Level Thickness Control of Single-Crystalline Zinc Oxide Nanosheets Enabled by Electrical Double-Layer Confinement, Langmuir, 33 (2017) 7708-7714.
[26] Z. Zhang, C. Carlos, Y. Wang, Y. Dong, X. Yin, L. German, K.J. Berg, W. Bu, X. Wang, Nucleation Kinetics and Structure Evolution of Quasi-Two-Dimensional ZnO at the Air–Water Interface: An In Situ Time-Resolved Grazing Incidence X-ray Scattering Study, Nano Letters, 22 (2022) 3040-3046.
[27] Z. Zhang, D. Ni, F. Wang, X. Yin, S. Goel, L.N. German, Y. Wang, J. Li, W. Cai, X. Wang, In vitro study of enhanced photodynamic cancer cell killing effect by nanometer-thick gold nanosheets, Nano Research, 13 (2020) 3217-3223.
[28] M.M. van der Sluijs, B.B.V. Salzmann, D. Arenas Esteban, C. Li, D. Jannis, L.C. Brafine, T.D. Laning, J.W.C. Reinders, N.S.A. Hijmans, J.R. Moes, J. Verbeeck, S. Bals, D. Vanmaekelbergh, Study of the Mechanism and Increasing Crystallinity in the Self-Templated Growth of Ultrathin PbS Nanosheets, Chemistry of Materials, 35 (2023) 2988-2998.
[29] E. Yamamoto, A. Suzuki, M. Kobayashi, M. Osada, Tailored synthesis of molecularly thin platinum nanosheets using designed 2D surfactant solids, Nanoscale, 14 (2022) 11561-11567.
[30] W. Janusz, E. Skwarek, Comparison of oxalate, citrate and tartrate ions adsorption in the hydroxyapatite/aqueous electrolyte solution system, Colloids and Interfaces, 4 (2020) 45.
[31] J. Owen, The coordination chemistry of nanocrystal surfaces, Science, 347 (2015) 615-616.
[32] S. Karanth, R. Iyyaswami, Mixed Surfactant-Based Reverse Micellar Extraction Studies of Bovine Lactoperoxidase, Journal of Surfactants and Detergents, 24 (2021) 255-267.
[33] V.t. Yadava, V. Padmanabhan, The crystal structure of ammonium tartrate, Acta Crystallographica Section B: Structural Crystallography and Crystal Chemistry, 29 (1973) 493-498.
[34] J.A. Rood, B.C. Noll, K.W. Henderson, Homochiral frameworks derived from magnesium, zinc and copper salts of l-tartaric acid, Journal of Solid State Chemistry, 183 (2010) 270-276.
[35] S. Neveu, A. Bee, M. Robineau, D. Talbot, Size-selective chemical synthesis of tartrate stabilized cobalt ferrite ionic magnetic fluid, Journal of colloid and interface science, 255 (2002) 293-298.
[36] J.J. De Yoreo, P.G. Vekilov, Principles of crystal nucleation and growth, Reviews in mineralogy and geochemistry, 54 (2003) 57-93.
[37] V.K. LaMer, R.H. Dinegar, Theory, production and mechanism of formation of monodispersed hydrosols, Journal of the american chemical society, 72 (1950) 4847-4854.
[38] F. Wang, J.-H. Seo, G. Luo, M.B. Starr, Z. Li, D. Geng, X. Yin, S. Wang, D.G. Fraser, D. Morgan, Z. Ma, X. Wang, Nanometre-thick single-crystalline nanosheets grown at the water–air interface, Nature Communications, 7 (2016) 10444.
[39] Y. Wu, Y. Li, J. Gao, Q. Zhang, Recent advances in vacancy engineering of metal-organic frameworks and their derivatives for electrocatalysis, SusMat, 1 (2021) 66-87.

[40] S. Gao, Y. Sun, F. Lei, L. Liang, J. Liu, W. Bi, B. Pan, Y. Xie, Ultrahigh Energy Density Realized by a Single-Layer β-Co(OH)2 All-Solid-State Asymmetric Supercapacitor, Angewandte Chemie International Edition, 53 (2014) 12789-12793.
[41] Z. Liang, C. Zhang, Y. Xu, W. Zhang, H. Zheng, R. Cao, Dual Tuning of Ultrathin α-Co(OH)2 Nanosheets by Solvent Engineering and Coordination Competition for Efficient Oxygen Evolution, ACS Sustainable Chemistry & Engineering, 7 (2018) 3527-3535.
[42] C.C.L. McCrory, S. Jung, I.M. Ferrer, S.M. Chatman, J.C. Peters, T.F. Jaramillo, Benchmarking Hydrogen Evolving Reaction and Oxygen Evolving Reaction Electrocatalysts for Solar Water Splitting Devices, Journal of the American Chemical Society, 137 (2015) 4347-4357.
[43] C.C.L. McCrory, S. Jung, J.C. Peters, T.F. Jaramillo, Benchmarking Heterogeneous Electrocatalysts for the Oxygen Evolution Reaction, Journal of the American Chemical Society, 135 (2013) 16977-16987.